Journal of Applied Geophysics 78 (2012) 85–93

Contents lists available at ScienceDirect

Journal of Applied Geophysics

journal homepage: www.elsevier.com/locate/jappgeo

Using stochastic crosshole seismic velocity tomography and Bayesian simulation to estimate Ni grades: Case study from Voisey's Bay, Canada

L. Perozzi [a,*], E. Gloaguen [a], S. Rondenay [b], G. McDowell [c]

[a] INRS, Centre Eau Terre Environnement, 490 de la Couronne, Quebec, Qc, Canada G1K 9A9
[b] Department of Earth, Atmospheric and Planetary Sciences, Massachusetts Institute of Technology, 77 Massachusetts Avenue, Cambridge, MA 02139, USA
[c] Vale Inco, Sudbury, Ontario, Canada

ARTICLE INFO

Article history:
Received 1 November 2010
Accepted 27 June 2011
Available online 13 July 2011

Keywords:
Crosshole seismic tomography
Seismic inversion
Grade estimation
Voisey's Bay

ABSTRACT

Modeling of grades is a key step and the major source of error in appraisal stage of mining projects. We used a geostatistical approach to explicitly integrate seismic travel time data, as well as acoustic and core logging data into the estimation of nickel grades in the Voisey's Bay deposit. Firstly, the crosshole seismic travel times are inverted using a stochastic tomographic algorithm. This algorithm allows for the inclusion of acoustic log data and seismic covariance into the inverse problem, leading to high-resolution velocity tomographic images of the orebody. Secondly, grade realizations are generated using a Bayesian sequential Gaussian simulation algorithm, which integrates the ore grades measured on the core logs and the previously inverted tomographic data. The application of the presented method to the Voisey's Bay deposit yields an improved knowledge of the geology setting and generates grade models with realistic spatial variability compared to conventional methods.

1. Introduction

In the mining industry, building an interpretative model of a deposit is the first step to move from resource to reserve, as it forms the basis for the resource estimation process. Since the primary source of information comes from drill-hole samples, the interpretative model of the deposit is highly dependent on the spatial distribution of these samples. However, most of the new discoveries are located at depths between 500 m and 2000 m. At these depths, the costs of drilling increase dramatically and the ability of the drill-holes to accurately sample the mineralization decreases, such that increased depth of drilling limits the quality of the information. High resolution geophysical methods such radio-frequency (0.1 − 5 MHz) electromagnetic methods (Fullagar et al., 2000), borehole radar tomography (Bellefleur and Chouteau, 2001; Zhou and Fullagar, 2001) or seismic tomography (Enescu et al., 2002; Wong, 2000; Xu and Greenhalgh, 2010) provide the geologist with new information that can be incorporated into the process of orebody modeling. In addition, it has been shown that sonic logs can be used to constrain seismic tomography between drill-holes, resulting in a significant increase in the accuracy of the tomographic images (Gloaguen et al., 2007; Perozzi et al., 2010).

Geostatistical simulations are increasingly used for orebody modeling and mine planning in both open-pit and underground mining ventures (David, 1988; Dimitrakopoulos, 1998; Journel, 1974; Journel and Huijbregts, 1978). Drill-holes data are often complemented with other secondary, or so-called “soft” data (e.g., data from geophysics, geotechnics and geochemistry) to improve the understanding of the deposit model. In this framework, an optimal estimate of the mineralization grades, and thus the available resources, is likely achieved by integrating these different types of complementary data. The importance of integrating “hard” and “soft” spatial data has long been recognized in the petroleum industry, where reservoir properties such as permeability and porosity need to be inferred from a limited number of drill-holes (Doyen, 1988; Journel and Alabert, 1990; Le Ravalec-Dupin et al., 2001; Xu et al., 1992). Integrated modeling has also been used in the mining industry in ore reserve estimation (David, 1988; Journel and Huijbregts, 1978). Recently, integrated techniques have been used to merge core log data with crosshole tomographic data for orebody modeling (Dimitrakopoulos and Kaklis, 2001).

The present study describes a novel approach for integrating crosshole seismic velocity tomography with Ni grade data measured on diamond drill-hole core samples to better estimate the spatial variability of the ore grade. The benefit of this approach lies in the use of a kernel multivariate density estimator of the joint distribution between velocity and Ni grade data, to evaluate the likelihood function. The likelihood is used to obtain a conditional probability of Ni grades for a given velocity value.

2. Geological and geophysical settings

The Voisey's Bay intrusion belongs to the Nain Plutonic Suite and transects the collisional boundary between the Proterozoic Churchill Province to the west and the Archean Nain Province to the east (Fig. 1a). The Voisey's Bay Ni–Cu–Co deposit is associated with two 1.334 Ga troctolite intrusive chambers, the upper Eastern Deeps and

* Corresponding author.
E-mail address: lorenzo.perozzi@ete.inrs.ca (L. Perozzi).

0926-9851/$ – see front matter
doi:10.1016/j.jappgeo.2011.06.036

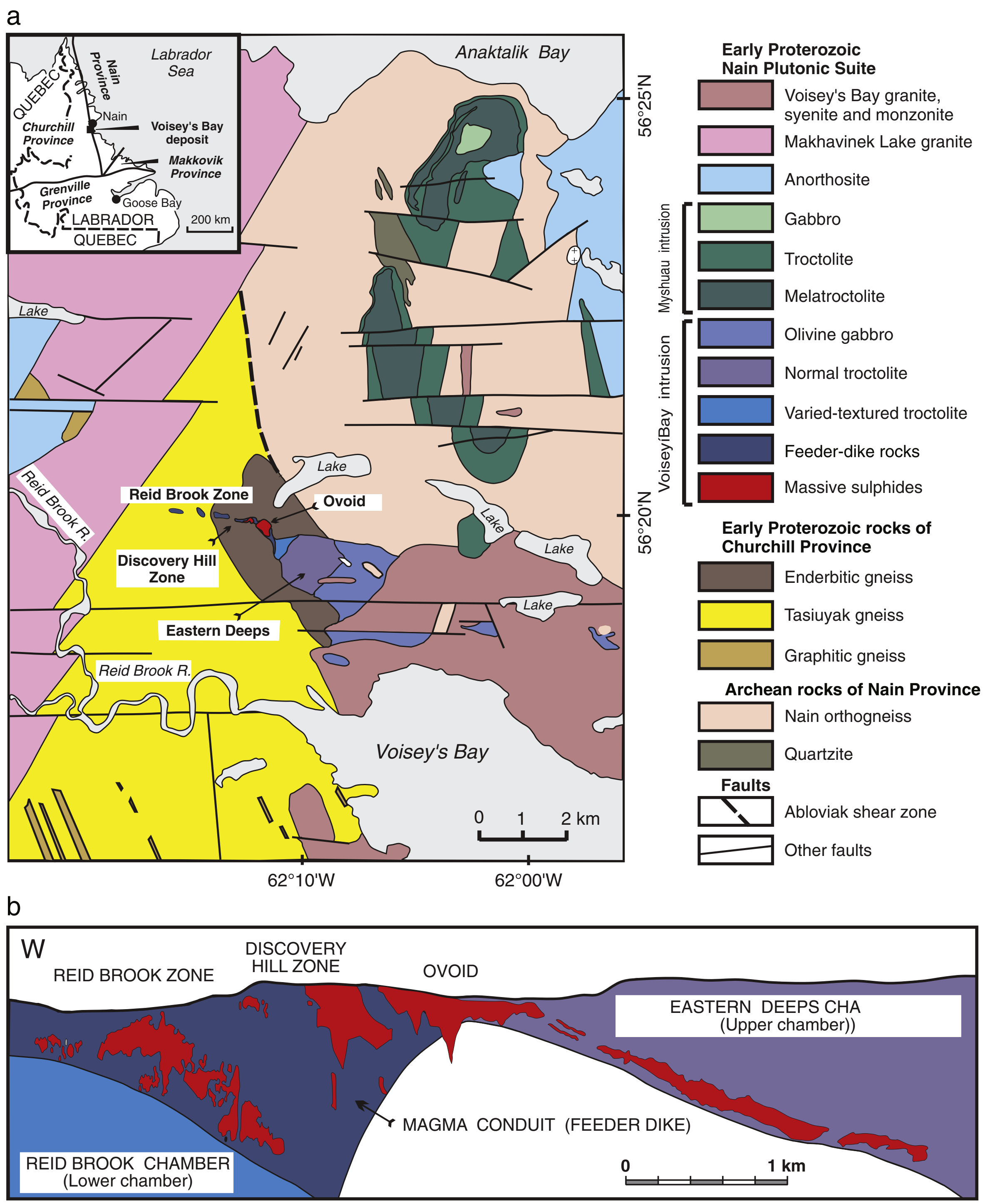

Fig. 1. a) Regional geology of Voisey's Bay; b) Generalized longitudinal cross-section of the Voisey's Bay deposit (modified from Naldrett and Li (2007)).

the lower Reid Brook (Fig. 1b), which are connected by a 10 to 100 m thick dyke (Naldrett and Li, 2007). The complexity of the geological settings and the spatial variability of mineralization both contribute to high uncertainties with regards to the shape and the grades of the deposit between the boreholes. A detailed description of the geology of Voisey's Bay can be found in Evans-Lamswood et al. (2000); Naldrett and Li, (2007). The mineralization in Voisey's Bay deposit is composed of massive, semimassive, and disseminated pyrrhotite, pentlandite, and chalcopyrite. The seismic property (P-wave velocity) of those sulfides as well as of most common silicate rocks is well known from laboratory studies (Birch, 1960; Christensen, 1982; Salisbury et al., 1996, 2000, 2003). These study shows that the properties of mixed and disseminated sulfides lie along simple mixing lines connecting the properties of end-member sulfides and felsic or mafic gangue. Thus, velocities increase dramatically with increasing pyrite content, but they actually decrease with increasing pyrrothite, chalcopyrite and pentlandite content along trend which can be calculated using the time average relationship of Wyllie et al. (1958).

A crosshole seismic tomography survey that recovers seismic velocities was thus deployed at the Voisey's Bay deposit in order to refine the geological model and better estimate the spatial distribution of grades.

3. Methodology

In this section, we introduce the methodology used in this study. Firstly, we describe the crosshole seismic tomography inversion and then the integration of the seismic velocities with grades.

3.1. Crosshole seismic stochastic tomography

Crosshole seismic tomography offers means to investigate elastic properties of the rock mass between two or more boreholes. This technique has been developed and applied in the last 30 years in a number of settings worldwide (Gustavsson et al., 1984). In Canada, crosshole seismic tomography applied to mining has been reported by Cochrane et al. (1999); Cosma and Enescu (2003); Maxwell and Young (1993); Wong (2000).

Crosshole seismic traveltime tomography is based on the assumption that the energy travels from a source (lowered into a borehole) to a receiver (lowered into another neighboring borehole) along a well-constrained ray path. Fig. 2 shows the acquisition geometry employed in our experiment and the resulting ray coverage. The source borehole (542) is on the left side of the figure, and the receiver borehole (540) is on the right side. A common approach to approximate wave paths is to use the ray approximation, in which the energy is assumed to travel between two points along well-defined curves. A ray is thus defined as the curve that connects a source to a receiver, and lies perpendicular to the wave front at any given point in space and time (Berryman, 1991). In ray-based tomography, the model space between boreholes is discretized in a series of cells of constant velocity. For each source-receiver pair, the length of each segment of ray path that crosses a cell is computed. The traveltime t in each cell is simply the length of the path in the cell multiplied by the cell's slowness (reciprocal of the velocity),

$$Ls = t \tag{1}$$

where L describe the geometry of the rays, s is the slowness. In order to linearize the problem, we assume that the ray path does not change (to first order) with small changes in model velocity distribution. Unfortunately, borehole tomography is a well known ‘ill-posed’

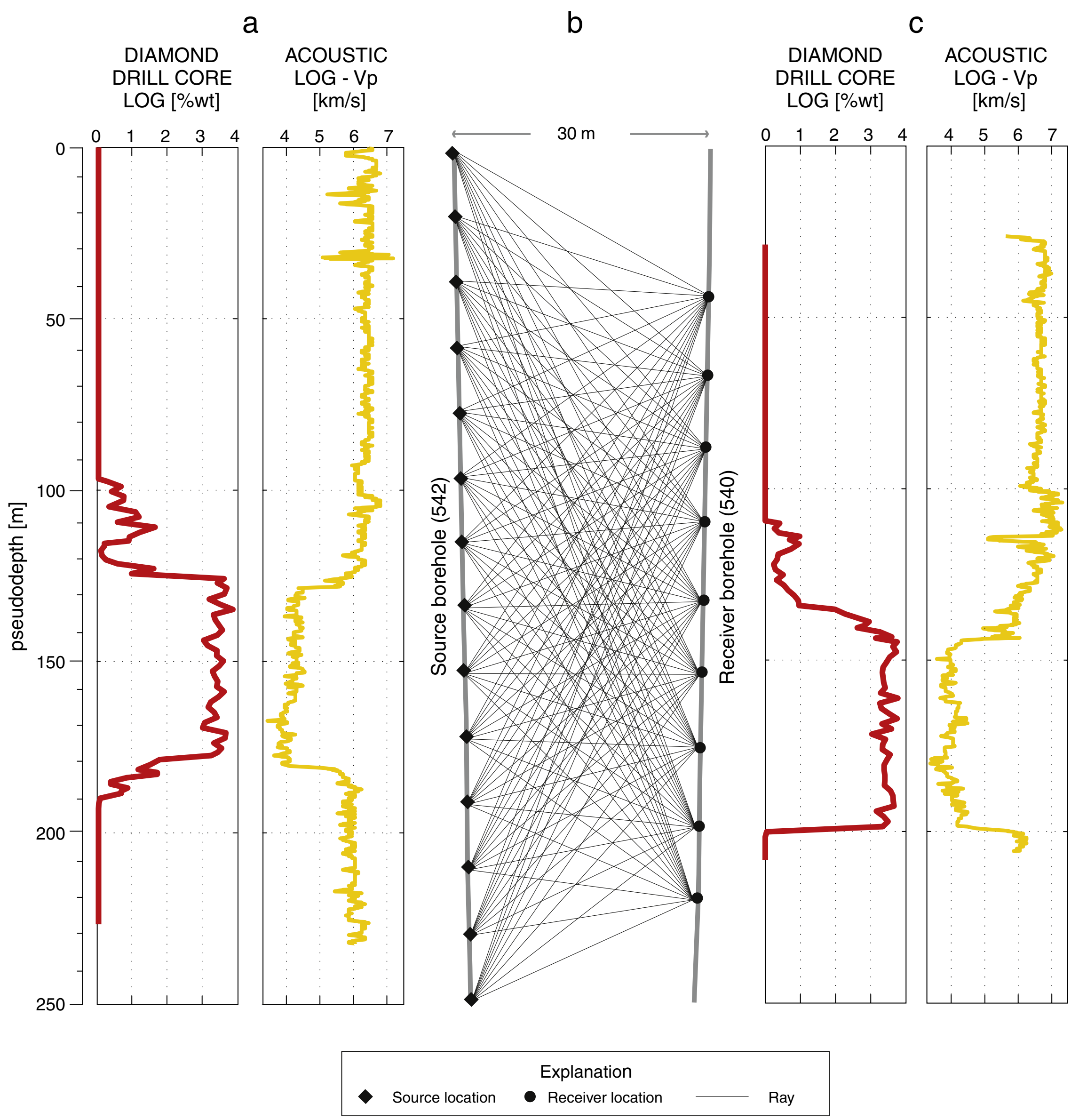

Fig. 2. a) Logs from the borehole 542. Red: Ni grades measured on core samples. Green: acoustic log showing the V_p along the hole; b) acquisition geometry for seismic tomography showing partial ray coverage between boreholes pair 542 (Tx) and 540 (Rx); c) the same as a) for the Rx borehole.

problem (Berryman, 1991). Thus L is not directly invertible. Classical Least Squares based algorithms such as LSQR (Least Squares QR factorization) (Paige and Saunders, 1982) are widely used in seismic tomography. The LSQR algorithm converges quickly and is particularly effective for sparse matrices. However, the convergence criteria must be carefully chosen to avoid the algorithm iterating on noise.

More recently, geostatistical approaches for linear inverse problems became widespread (Gloaguen et al., 2005, 2007; Hansen and Mosegaard, 2008; Hansen et al., 2006). In particular, Gloaguen et al. (2005, 2007) developed a new type of tomographic algorithm that combines geostatistical simulation and tomography in the same process. The algorithm is based on the linear relation between slowness and travel time (cf. Eq. (1)) and the fact that their covariance matrices are also linearly related,

$$cov(t,t) = L\ cov(s,s)L^T + C_0 \quad (2)$$

where $cov(t,t)$ is the travel time covariance matrix, $cov(s,s)$ is the slowness parameter covariance matrix and C_0 is the travel time error covariance matrix. An important step of stochastic tomography is the covariance modeling (Gloaguen et al., 2005). The slowness covariance $cov(s,s)$ can be modeled by choosing a model function whose parameters are estimated using the experimental covariances of the travel times. When an acceptable slowness covariance model is obtained, the stochastictomographic inversion of the slowness field is computed. Because the true velocity field is not known, the first tomographic iteration is performed using straight ray approximation. Of course, the straight ray is not a satisfying approximation. Thus, the linear system has to be solved iteratively, computing curved ray at each iteration. In our case, three curved ray iterations were done. In addition, acoustic logs along the boreholes can be used as constraints to decrease the variance of the estimated velocity (Gloaguen et al., 2007; Perozzi et al., 2010).

3.2. Integration of seismic tomographic images and grades

Random field theory (Christakos, 1992) can account for multiple spatial variables and yields robust estimates of a primary attribute (ore grade in our case) by using a number of secondary variables (for instance geophysical data). Several approaches for the inclusion of auxiliary data in inverse problems have been proposed in geosciences (Cassiani et al., 1998; Deutsch and Journel, 1998; Dimitrakopoulos and Kaklis, 2001; Journel and Huijbregts, 1978). Among them, Bayesian sequential Gaussian simulation (BSGS) provides a framework to update a prior distribution by using the joint probability density function between a primary variable (here, the Ni grades θ_n) and secondary variable (here, the seismic velocity V_p). BSGS has previously been used to map porosity from seismic data (Doyen et al., 1996) to predict reservoir thickness under tuning conditions (Gastaldi et al., 1998) and to characterize heterogeneous aquifer (Dubreuil-Boisclair et al., 2011). In this method, it is assumed that the multivariate statistical relationship between ore grade (θ_n) and seismic velocities (V_p) field, measured along boreholes, can be described by a spatially invariant joint probability distribution. The non-parametric kernel density estimation method (Parzen, 1962) is used to estimate this probability distribution function. The BSGS is applied by repeating 4 steps as illustrated in Fig. 3. First, a grid cell is randomly selected to be the object of the simulation of model parameter θ_n (a). Second, the prior θ_n distribution for each cell is obtained by simple kriging under Gaussian hypothesis using known θ_n values (b). Third, we compute the likelihood by extracting a slice of the joint probability distribution (Fig. 4b) for the grades corresponding to the measured seismic velocity at the selected grid cell. The likelihood function determines the range of possible grade values consistent with the observed velocity tomography (c). Fourth, we calculate the posterior grade distribution by calculating the product of the prior model distribution and the likelihood function (d). Steps

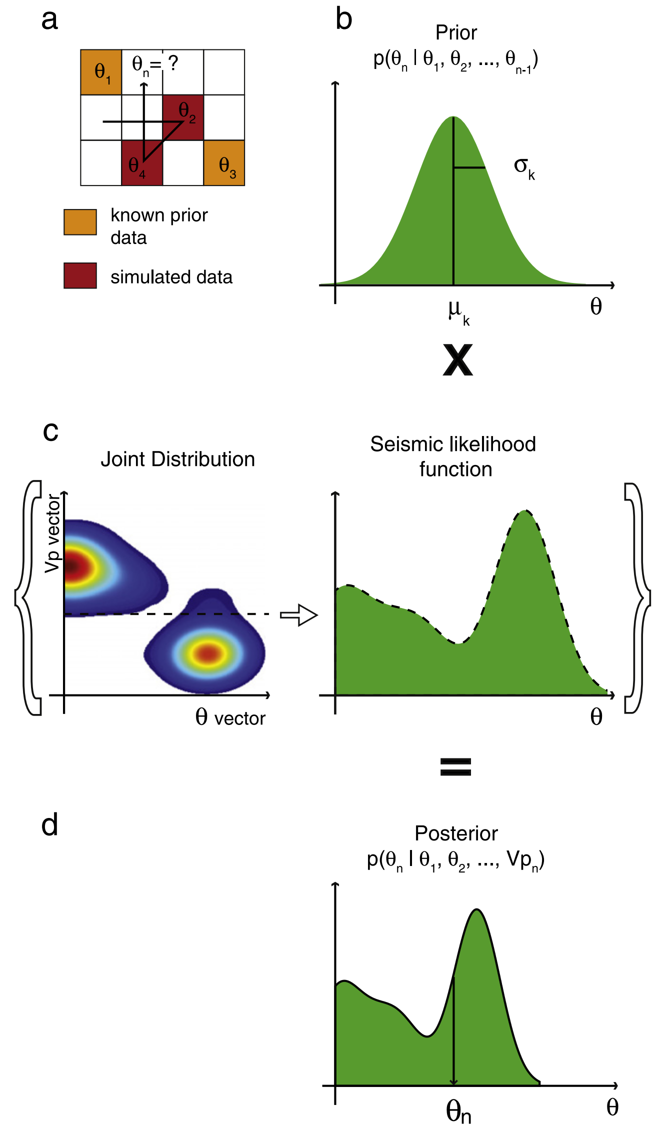

Fig. 3. Description of the BSGS approach. Look in the text for the description (modified from Gastaldi et al. (1998)).

(a) to (d) are repeated until all the grid cells are simulated, taking into account, for every new cell grid, the values previously simulated.

4. Acquisition parameters and data at Voisey's Bay deposit

Vibrometrics was contacted by Inco Ltd to acquire crosshole seismic data between a number of boreholes during the second phase of the Eastern Deeps delineation program. The spacing between the boreholes pair 542–540, retained for this study is 30 m (Fig. 2b). The apparatus used at Voisey's Bay consists of a piezoelectric source based on the Swept Impact Seismic Technique (SIST) (Park et al., 1996) and a string of 24 hydrophones. The source employed at Voisey's Bay produce sweeps of high voltage (6000 V) pulses during 20 to 30 s. The frequency band employed was 100 — 3000 Hz. More details about the apparatus and on the tomographic data can be found in Cosma and Enescu (2003) and Enescu et al. (2002).

The seismic velocities V_p of the formation adjacent to the boreholes were also measured with acoustic logging probes. Analysis of Ni and other mineral grades on core samples along boreholes were also logged.

Fig. 2 shows both the acoustic logs (P-wave velocity) and core logs (nickel ore grades) for boreholes 542 (Fig. 2a) and 540 (Fig. 2c)

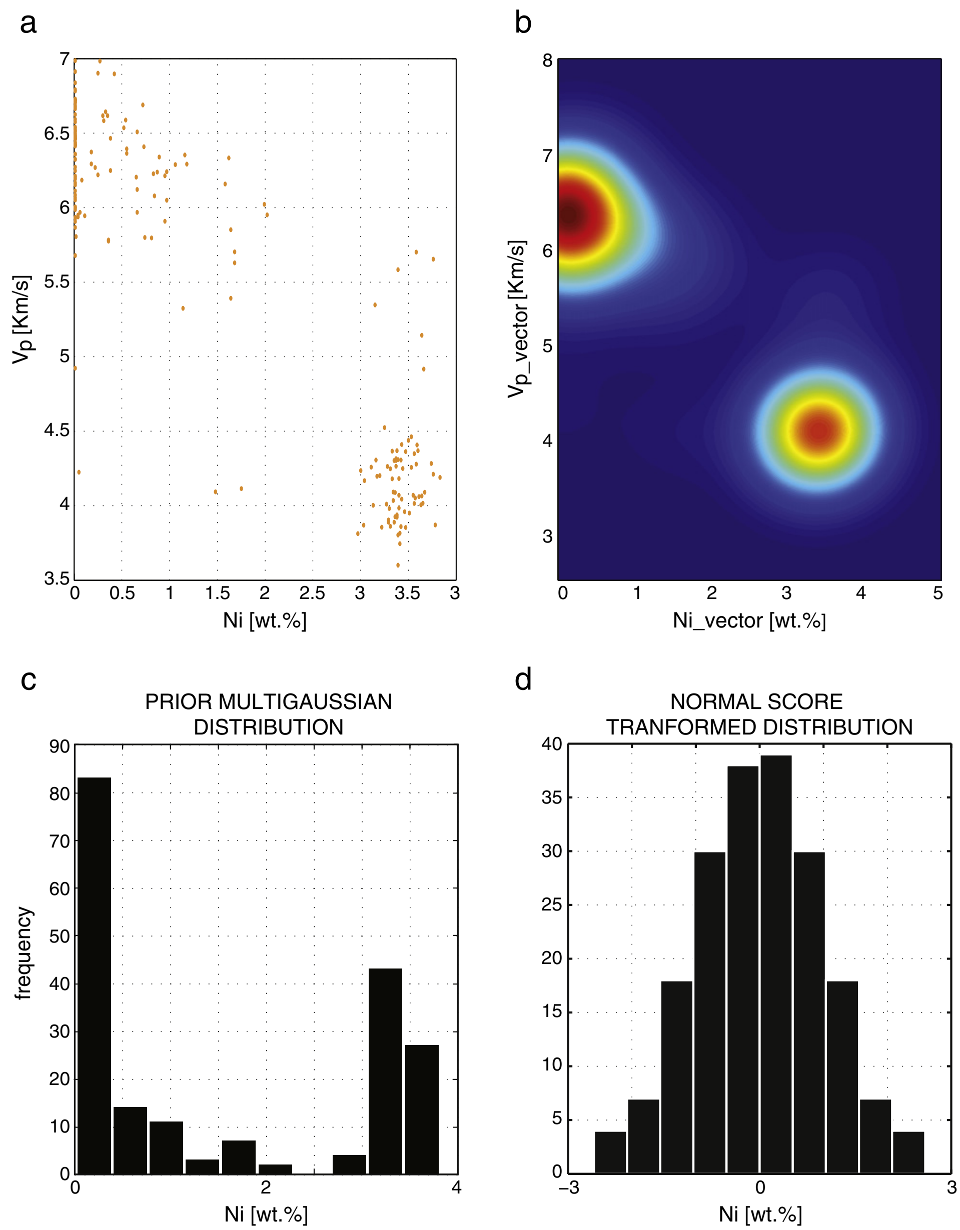

Fig. 4. a) Scatter plot between V_p et Ni grades (θ_n); b) Joint probability function between V_p and Ni grades (θ_n); b) Ni grade distribution along boreholes before n-score transformation; c) Ni grade distribution along boreholes after n-score transformation.

as well as the crosshole seismic survey geometry between the source borehole (542) and the receiver borehole (540) (Fig. 2b). The latter shows simplified ray coverage between the two boreholes; the total number of rays is more than 20,000. A direct relationship between a decrease in V_p response and an increase in sulfide grade is clearly displayed in both Fig. 2a and c. Many variables in the Earth Sciences, such as grades measured on core samples, show an asymmetric distribution with a few very large values (positive skewness). In order to estimate the a priori distribution in the sequential Gaussian simulation framework, a transformation of the original grade data distribution into normally distributed grade data is needed, which is achieved by normal score transform, (Deutsch and Journel, 1998). At each cell to be simulated, back transformation of the a priori distribution into the original space distribution is then applied. This is done by sampling the normal distribution and back-transforming each samples at a time. Fig. 4b shows the prior asymmetric distribution and Fig. 4c shows the normal scores distribution.

5. Results

5.1. Stochastic crosshole seismic tomography

The survey covers an area measuring 232×30 m^2. It was divided into a grid of 1.5×1.5 m^2 cells, leading to a total of 3496 cell values to estimate. The estimated slowness covariance model is an exponential model with ranges equal to 60 m across and 10 m along boreholes. The slowness variance is found to be $0.002(\mathrm{s/km})^2$ and the nugget effect for travel times is equal to $0.1\mathrm{s}^2$. Fig. 5 shows the seismic velocities. The inversion process has been computed with the *bh_tomo* package (Giroux et al., 2007) in the Matlab programming environment. The source (542) and the receiver (540) borehole locations are enhanced with a black contour line. Fig. 5a shows the "best" simulated realization obtained after gradual deformation of 32 stochastic realizations. In the gradual deformation method (GD) (Hu, 2002; Le Ravalec-Dupin and Nœtinger, 2002), the 32 realizations are combined sequentially, two at time, with weights chosen as to minimize the gap between computed

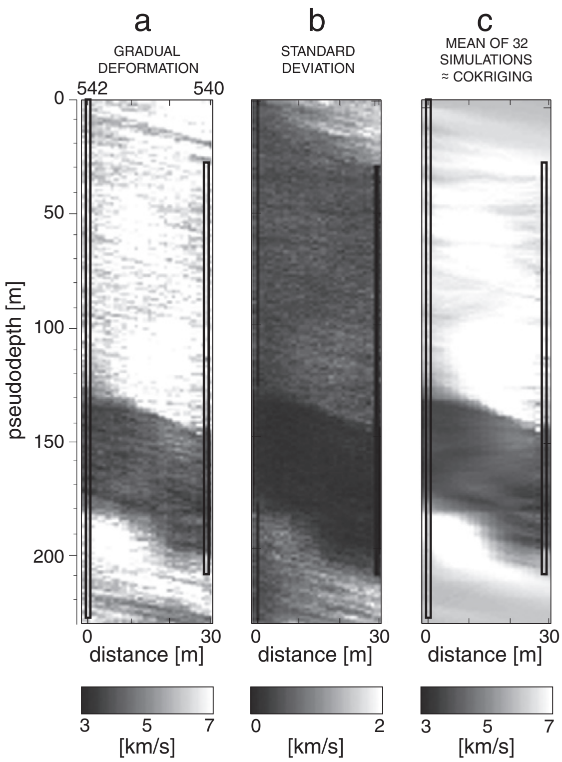

Fig. 5. Stochastic seismic tomography inversion (black rectangles on the sides denotes the boreholes): a) the "best" simulated realization obtained after gradual deformation of 32 stochastic realizations; b) the standard deviation of all 32 realizations; c) the mean of all 32 realizations.

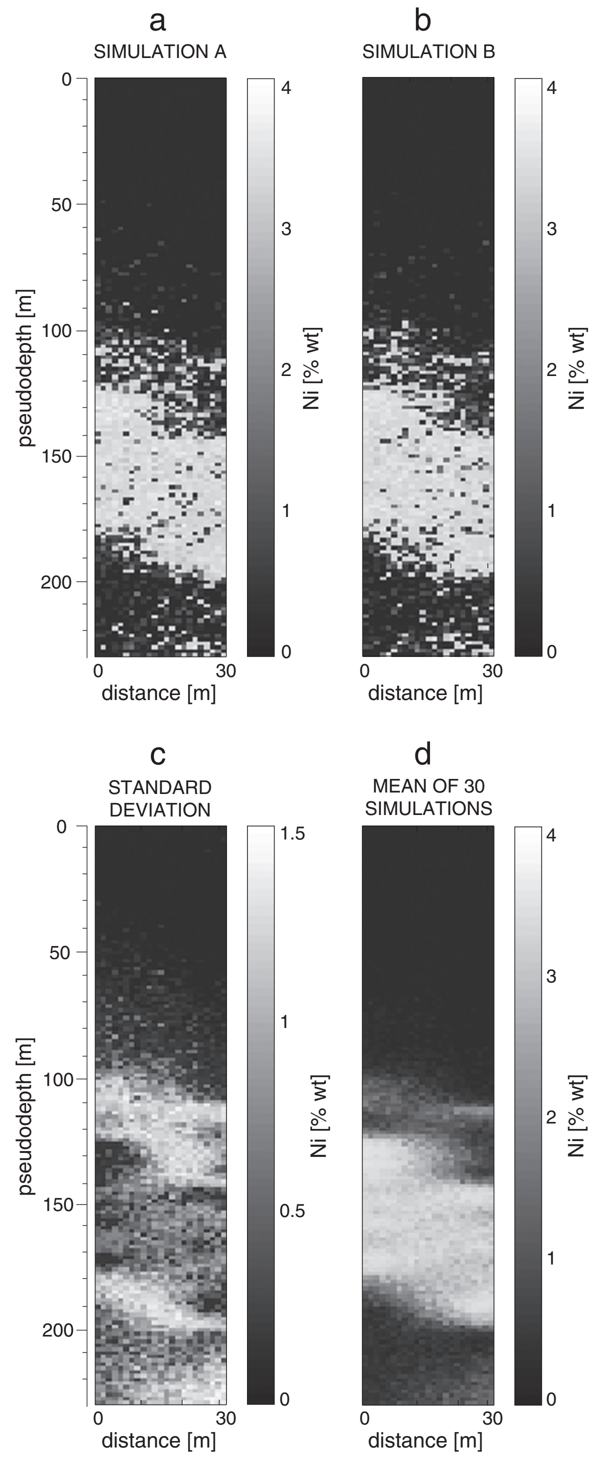

Fig. 6. Sequential Gaussian simulation for nickel grades. The different panels show (a–b) two simulations among 30 realizations, (c) the standard deviation of the 30 realizations and (d) the mean of the 30 realizations.

and measured travel times. The gradual deformation method enables the identification of stable and well-defined features present in most retained realizations. The results obtained from GD method will be used as the reference V_p model for the BSGS algorithm. The choice of calculating 32 realizations is a compromise between computing time and variability between realizations. The uncertainty on the results is inferred from the standard deviation of the model distribution, as shown in Fig. 5b. Standard deviation values are relatively small everywhere (<1 km/s) except at the top and the bottom of the borehole 540 where there is no ray coverage. The map of standard deviation gives a visual assessment of the uncertainty associated with the velocity estimates and thus the robustness of the features in the image. The uncertainty is null where constraints on velocity are available (along boreholes) and is higher in high velocity area compared to low velocity areas. Taking the mean of the 32 stochastic realizations (Fig. 5c) yields a resulting model that is comparable to the model produced by cokriging.

Fig. 5a and c shows a 50 m thick zone of low velocity at a pseudo-depth of 150 m that exhibits a strong continuity between boreholes 542 and 540. The contrast with the velocity of the host rock is of the order of 3.5 km/s. The model resulting from the gradual deformation approach comprises two thin low-velocity zones at the top and the bottom of the receiver borehole (540). These are artifacts associated to regions of the model where ray coverage is limited or non-existent.

5.2. Standard sequential Gaussian simulation (SGS)

In this paragraph, we illustrate briefly the standard grade modeling technique based on grades measured along boreholes. Fig. 6 shows an example of a conventional sequential Gaussian simulation (SGS) of the grades between boreholes 542 and 540. As in our case we are dealing with non-Gaussian variables, a Gaussian transform has been applied to the well data and the simulation is conducted from the Normal score. This figure presents two randomly chosen realizations (a and b) among 30 realizations, the standard deviation (c) and the mean of 30 simulations for nickel grade (d). The massive sulfide body is clearly observed between the two boreholes. However, this method does not resolve precisely the limits of the deposit, as confirmed by the high standard deviation values obtained at the edges of the mineralized region (1.5 km/s, Fig. 6c). As shown above, an important issue that needs to be addressed in all SGS models of reserve estimation is the approach used to define the boundaries of the mineralization, since these boundaries define the region within which geostatistical modeling is applied. The outlines of the mineralized body (or wireframes) are traditionally traced manually on the basis of the grades measured on the drill cores. This approach is extremely time consuming and sometimes inaccurate due to the complex geometry of the ore bodies. Since manual methods are often associated with non-reproducible implementation, they can lead to high dilution of the minable units (Pan, 1995). For those reasons, the Bayesian approach has been proposed in this study.

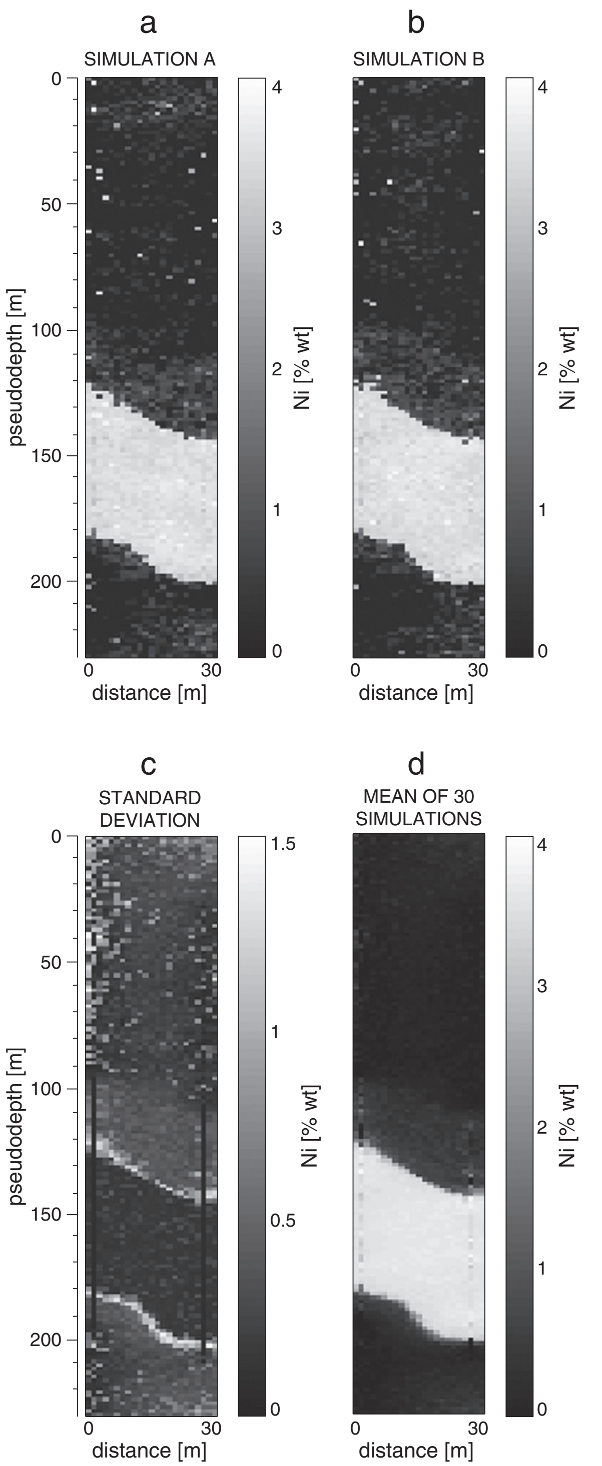

Fig. 7. Bayesian sequential Gaussian simulation (BSGS) for nickel grades between boreholes 540 (source) and 542 (receiver). The different panels show (a–b) two simulations among 30 realizations, (c) the standard deviation of the 30 realizations, and (d) the mean of the 30 realizations.

5.3. Bayesian sequential Gaussian simulation (BSGS)

The Bayesian sequential Gaussian simulation (BSGS) proposed in this paper (Fig. 7) is compared to the results obtained with a conventional sequential Gaussian simulation (Fig. 6). The V_p image obtained with the GD method presented above is used as reference image for the BSGS algorithm. Hence, at every pixel we know the optimal tomographic V_p. This value is used to obtain the Ni grade likelihood distribution from the kernel multivariate density estimator (Fig. 3c). Fig. 7 shows two randomly chosen realizations (a and b) among 30 simulations, the standard deviation (c) and the mean of 30 simulations for nickel grade (d). The choice to calculating 30 realizations arises from the fact that adding one more realization does not change considerably the variability between realizations. The massive sulfide zone is clearly observed. The values for nickel grades in Fig. 7a and b are quite high (≈ 4 wt.% of Ni). Fig. 7c shows that the uncertainty is close to zero except at the border of the mineralization. This can be explained by the fact that in the kernel, a value around 5 km/s gives almost the same probabilities to have Ni grades between $0-4$ wt.% (Fig. 4a). This high probability range of Ni grade obviously increases the variability between each realization. The mean of the 30 simulations shown in Fig. 7d gives a nickel grade model with values between 3 to 4 wt.% that is consistent with the values measured along boreholes.

5.4. Bayesian simulation without direct observation of grades along boreholes

The Bayesian simulation does not require the relation between grades and sonic logs to be assessed in every borehole. In fact, we assume that the relationship between nickel grade θ_n and V_p, built for a nearby boreholes pair is approximately the same in surrounding regions. Hence, we can build model grades for boreholes pair investigated by crosshole tomography by using the same non-parametric kernel density. Fig. 8 shows the tomography-based

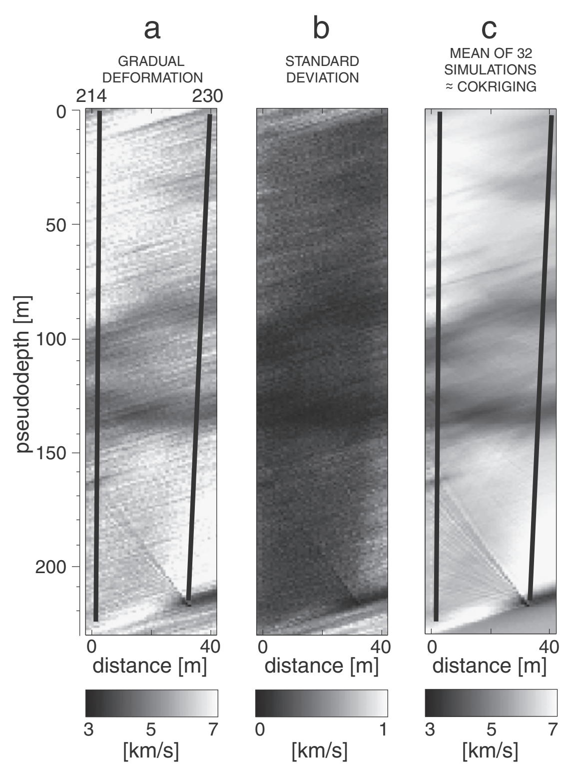

Fig. 8. Stochastic seismic tomography inversion (black rectangles on the sides denote the boreholes 214 (source) and 230 (receiver)): a) the “best” simulated realization obtained after gradual deformation of 32 stochastic realizations; b) the standard deviation of the 32 realizations; c) the mean of the 32 realizations.

velocities between boreholes 214 (source) and 230 (receiver) from the Eastern Deeps, obtained with the geostatistical inversions. As in Fig. 5, the gradual deformation (a), the standard deviation (b) and the mean of 32 simulations (c) are presented. A decay in V_p associated with a subhorizontal massive sulfide region is obvious. The standard deviation (Fig. 8b) shows that the uncertainty is generally low (<0.5 km/s) except for the zones where the ray coverage is poor (bottom of the receiver (230) borehole).

Even if we do not have access to the Ni grades measured on diamond core for boreholes pair 214–230, we are able to compute a BSGS by using the joint probability distribution function between V_p and θ_n built for the boreholes pair 542–540. The results are shown in Fig. 9. Two realizations (a and b), the standard deviation c) and the mean of 30 simulations (d) are presented. In Fig. 9d, the nickel zone is clearly visible, subhorizontal and continuous between boreholes at a pseudo-depth between 80 m and 140 m and its limits are well defined. The geometry is consistent with the geological model described in Naldrett and Li (2007). The uncertainty (Fig. 9c) is close to zero, except near the mineralization limits and, generally where the seismic velocities (Fig. 8) are around 5. This can be explained, as for the Fig. 7c, by the fact that in the joint probability function, a velocity around 5 km/s gives almost the same probabilities to have Ni grades between 0 − 4 wt.% (Fig. 4a). This high probability range of Ni grade obviously increases the variability between each realization.

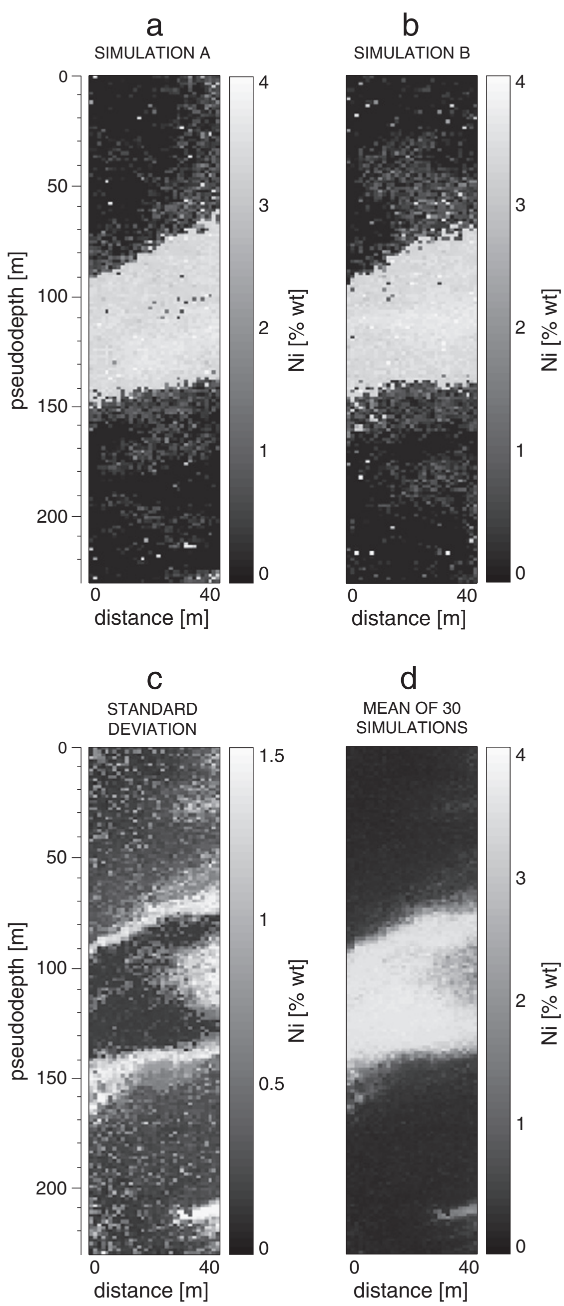

Fig. 9. Bayesian sequential Gaussian simulation (BSGS) for nickel grades between boreholes 214 (source) and 230 (receiver). As for Fig. 7, the different panels show (a–b) two simulations among 30 realizations, (c) the standard deviation of the 30 realizations, and (d) the mean of the 30 realizations.

6. Discussion and conclusion

The results obtained with crosshole seismic stochastic algorithm demonstrate the capacity of the method to give high resolution images for the mineralized body at Voisey's Bay. One benefit of this approach is that it is self-regularized. In addition, it enables the identification of stable and well-defined features present in every realization. In particular, geostatistical tomography allows a robust characterization of the low velocity zone, in this case associated with the mineralization zone (drastic decay of V_p). In addition, it has been shown that stochastic inversion can be constrained by sonic logs. It is obvious that we could retain other inversions method to obtain velocities between boreholes, but we chose this stochastic method as it preserves the whole amplitude range of the data. In the second part of the paper, the result obtained with the stochastic tomography inversion has been integrated with grades measured along boreholes using a BSGS for ultimately modeling nickel grades. This approach has been compared with a conventional SGS. The proposed method allows to build a model for Ni grades based on stochastic seismic tomography. The modeling of the in situ relationship between V_p and Ni grades is described by the kernel joint probability density function estimator. The results show that the proposed method is suitable for the grade simulations for two reasons: 1) since the geometry of the deposit is constrained by seismic tomography, the boundaries of the mineralization are better defined, leading to less dilution factors for blocks near or at boundaries; 2) the spatial distribution and estimation of nickel ore grade constrained by seismic tomography are in better agreement with the geological model of Eastern Deeps than the model obtained by conventional SGS. In addition, this method was shown to be applicable for the estimation of mineral grades between boreholes, even when direct observation along boreholes is not available. The method could be obviously applied to other economically worthwhile minerals estimation as Cu and Co. Other geophysical techniques such as EM, DC-resistivity or even seismic attenuation tomography could be included in the algorithm. Not only the boundaries of the mineralization could be better constrained, but also the geophysical parameter could be used to estimate the joint probability distribution, leading to more accurate results.

Acknowledgments

We are grateful to Vale Inco Ltd. for funding this research. We thank B. Giroux for precious suggestions and assistance with the processing of seismic tomography data and C. Dubreuil-Boisclair for the constructive suggestions. We also are grateful to T.M. Hansen and two anonymous reviewers for their constructive comments and suggestions.

References

Bellefleur, G., Chouteau, M., 2001. Massive sulphide delineation using borehole radar: tests at the McConnell nickel deposit, Sudbury, Ontario. Journal of Applied Geophysics 47, 45–61.
Berryman, J., 1991. Nonlinear inversion and tomography. Lecture Notes, Earth Resources Laboratory, pp. 126–131.
Birch, F., 1960. The velocity of compressional waves in rocks to 10 kilobars, part 1. Journal of Geophysical Research 65, 1083–1102.

Cassiani, G., Böhm, G., Vesnaver, A., Nicolich, R., 1998. A geostatistical framework for incorporating seismic tomography auxiliary data into hydraulic conductivity estimation. Journal of Hydrology 206, 58–74.

Christakos, G., 1992. Random Field Models in Earth Sciences. Academic Press, San Diego.

Christensen, N., 1982. Seismic velocities. In: Carmichael, R.S. (Ed.), Handbook of Physical Properties in Rocks, Vol II. CRC Press, pp. 1–228.

Cochrane, L., Thompson, B., McDowell, G., 1999. The application of geophysical methods to improve the quality of resource and reserve estimates. Exploration and Mining Geology 7, 63–75.

Cosma, C., Enescu, N., 2003. Ore delineation by crosshole seismics, transmission and reflection imaging at Voisey's Bay, Canada. Proceedings of the 7th International Symposium on Recent Advances in Exploration Geophysics.

David, M., 1988. Handbook of Applied Advanced Geostatistical Ore Reserve Estimation. Elsevier Science Pub. Co. Inc., New York, NY.

Deutsch, C., Journel, A., 1998. GSLIB: Geostatistical Software Library and User's Guide, Second edition. Oxford University Press.

Dimitrakopoulos, R., 1998. Conditional simulation algorithms for modelling orebody uncertainty in open pit optimisation. International Journal of Surface Mining, Reclamation, and Environment 12, 173–179.

Dimitrakopoulos, R., Kaklis, K., 2001. Integration of assay and cross-hole tomographic data in orebody modelling: joint geostatistical simulation and application at Mount Isa Mine, Queensland. Transactions of the Institutions of Mining and Metallurgy, Section B: Applied Earth Science 110, B33–B39.

Doyen, M., 1988. Porosity from seismic data: a geostatistical approach. Geophysics 53, 1263–1275.

Doyen, P., Den Boer, L., Pillet, W., 1996. Seismic porosity mapping in the Ekofisk Field using Bayesian stochastic simulation. EAGE Extended Abstracts.

Dubreuil-Boisclair, C., Gloaguen, E., Marcotte, D., Giroux, B., 2011. Heterogeneous aquifer characterization from ground-penetrating radar tomography and borehole hydrogeophysical data using nonlinear Bayesian simulations. Geophysics 76, J13–J25.

Enescu, N., McDowell, G.M., Cosma, C., Bell, C., 2002. Crosshole seismic investigations at Voisey's Bay, Canada. SEG Technical Program Expanded Abstracts 21, 1472–1475.

Evans-Lamswood, D.M., Butt, D., Jackson, R.S., Lee, D., Muggridge, M., Wheeler, R., Wilton, D., 2000. Physical controls associated with the distribution of sulfides in the Voisey's Bay Ni–Cu–Co deposit, Labrador. Economic Geology 95, 749–769.

Fullagar, P., D.W., L., Zhang, P., Calvert, A., Wu, Y., 2000. Radio tomography and borehole radar delineation of the McConnell nickel sulfide deposit, Sudbury, Ontario, Canada. Geophysics 65, 1920–1930.

Gastaldi, C., Roy, D., Doyen, P., Boer, L.D., 1998. Using Bayesian simulations to predict reservoir thickness under tuning conditions. The Leading Edge 17, 539.

Giroux, B., Gloaguen, E., Chouteau, M., 2007. *bh_tomo*—a Matlab borehole georadar 2D tomography package. Computers and Geosciences 33, 126–137.

Gloaguen, E., Marcotte, D., Chouteau, M., Perroud, H., 2005. Borehole radar velocity inversion using cokriging and cosimulation. Journal of Applied Geophysics 57, 242–259.

Gloaguen, E., Marcotte, D., Giroux, B., Dubreuil-Boisclair, C., Chouteau, M., Aubertin, M., 2007. Stochastic borehole radar velocity and attenuation tomographies using cokriging and cosimulation. Journal of Applied Geophysics 62, 141–157.

Gustavsson, M., Israelson, H., Ivansson, S., Moren, P., Pihl, J., 1984. An experiment with the seismic crosshole method in an iron mine. The Leading Edge 3, 143–145.

Hansen, T.M., Mosegaard, K., 2008. Visim: sequential simulation for linear inverse problems. Computers and Geosciences 34, 53–76.

Hansen, T.M., Journel, A.G., Tarantola, A., Mosegaard, K., 2006. Linear inverse Gaussian theory and geostatistics. Geophysics 71, R101–R111.

Hu, L.Y., 2002. Combination of dependent realizations within the gradual deformation method. Mathematical Geology 34, 953–963.

Journel, A., 1974. Geostatistics for conditional simulation of ore bodies. Economic Geology 69, 673–687.

Journel, A., Alabert, G., 1990. New method for reservoir mapping. Journal of Petroleum Technology 42, 212–218.

Journel, A., Huijbregts, C., 1978. Mining Geostatistics. Academic Press, New York.

Le Ravalec-Dupin, M., Nœtinger, B., 2002. Optimization with the gradual deformation method. Mathematical Geology 34, 125–142.

Le Ravalec-Dupin, M., Hu, L., Noetinger, B., 2001. Stochastic reservoir modeling constrained to dynamic data: local calibration and inference of structural parameters. SPE Journal 6, 25–31.

Maxwell, S., Young, R., 1993. Seismic imaging of blast damage. International Journal of Rock Mechanics and Mining Sciences and 30, 1435–1440.

Naldrett, A., Li, C., 2007. The Voisey's Bay deposit, Labrador, Canada. Mineral deposits of Canada: A synthesis of major deposit types, district metallogeny, the evolution of geological provinces and exploration methods. In: Goodfellow, Wayne D. (Ed.), Special Publication, 5. Geological Association of Canada, Mineral Deposits Division. 1,068 pp.

Paige, C.C., Saunders, M.A., 1982. LSQR: an algorithm for sparse linear equations and sparse least squares. ACM Transactions on Mathematical Software 8, 43–71.

Pan, G., 1995. Practical issues of geostatistical reserve estimation in the mining industry. CIM Bulletin 88, 31–37.

Park, C., Miller, R., Steeples, D., Black, R., 1996. Swept impact seismic technique (SIST). Geophysics 61, 1789–1803.

Parzen, E., 1962. On estimation of a probability density function and mode. Ann. Math. Statist. 33, 1065–1076.

Perozzi, L., Gloaguen, E., Rondenay, S., Leite, A., McDowell, G., Wheeler, R., 2010. Using stochastic borehole seismic velocity tomography and Bayesian simulation to estimate Ni, Cu and Co grades. EAGE Extended Abstracts.

Salisbury, M., Milkereit, B., Bleeker, W., 1996. Seismic imaging of massive sulfide deposits: part I. Rock properties. Economic Geology 91, 821–828.

Salisbury, M., Milkereit, B., Ascough, G., Adair, R., Matthews, L., Schmitt, D., Mwenifumbo, J., Eaton, D., Wu, J., 2000. Physical properties and seismic imaging of massive sulfides. Geophysics 65, 1882–1889.

Salisbury, M., Harvey, C., Matthews, L., 2003. The acoustic properties of ores and host rocks in hardrock terranes. In: Eaton, D., Milkereit, B., Salisbury, M. (Eds.), Hardrock Seismic Exploration: Society of Exploration Geophysicists: Geophysical Development Series, 10, pp. 9–19.

Wong, J., 2000. Crosshole seismic imaging for sulfide orebody delineation near Sudbury, Ontario, Canada. Geophysics 65, 1900–1907.

Wyllie, M.R.J., Gregory, A.R., Gardner, G.H.F., 1958. An experimental investigation of factors affecting elastic wave velocities in porous media. Geophysics 23, 459–493.

Xu, K., Greenhalgh, S., 2010. Ore-body imaging by crosswell seismic waveform inversion: a case study from Kambalda, Western Australia. Journal of Applied Geophysics 70, 38–45.

Xu, W., Tran, T., Srivastava, R., Journel, A., 1992. Integrating seismic data in reservoir modeling: the collocated cokriging alternative. Proceedings—SPE Annual Technical Conference and Exhibition Omega, pp. 833–842.

Zhou, B., Fullagar, P., 2001. Delineation of sulphide ore-zones by borehole radar tomography at Hellyer Mine, Australia. Journal of Applied Geophysics 47, 261–269.